Dependence of Contextual Modulation in Macaque V1 on Interlaminar Signal Flow

Shude Zhu[1], Yu Jin Oh[1], Ethan Trepka[1], Xiaomo Chen[1,2], Tirin Moore[1*]

Author affiliations:

[1]Department of Neurobiology and Howard Hughes Medical Institute, Stanford University School of Medicine, Stanford, CA 94305, USA.

[2]Center for Neuroscience, Department of Neurobiology, Physiology, and Behavior, UC Davis, Davis, CA 95618, USA.

***Correspondence:** tirin@stanford.edu

Abstract

In visual cortex, neural correlates of subjective perception can be generated by modulation of activity from beyond the classical receptive field (CRF). In macaque V1, activity generated by nonclassical receptive field (nCRF) stimulation involves different intracortical circuitry than activity generated by CRF stimulation, suggesting that interactions between neurons across V1 layers differ under CRF and nCRF stimulus conditions. We measured border ownership modulation within large populations of V1 neurons. We found that neurons in single columns preferred the same side of objects located outside of the CRF. In addition, we found that interactions between pairs of neurons situated across feedback/horizontal and input layers differed between CRF and nCRF stimulation. Furthermore, the magnitude of border ownership modulation was predicted by greater information flow from feedback/horizontal to input layers. These results demonstrate that the flow of signals between layers covaries with the degree to which neurons integrate information from beyond the CRF.

Introduction

The classical receptive field (CRF) defines the region of the sensory periphery where appropriate stimulation evokes a spiking response in a neuron(Hartline, 1938, Alonso and Chen, 2009). Those evoked responses are largely driven by feedforward inputs from earlier stages of sensory processing. In macaque primary visual cortex (V1), neuronal activity is largely determined by ascending input from the dorsal lateral geniculate nucleus (dLGN) which arrives principally in layers 4Cα, 4Cβ and 6(Hubel and Wiesel, 1972, Hendrickson et al., 1978, Blasdel and Lund, 1983, Callaway, 1998, Callaway, 2004). However, considerable evidence has established that the responses of sensory cortical neurons are also robustly influenced by stimulation concurrently presented outside of the CRF(Allman et al., 1985, Fitzpatrick, 2000, Albright and Stoner, 2002, Roelfsema, 2006, Angelucci et al., 2017). Specifically, whereas stimulation outside of the CRF alone fails to evoke spiking responses, such stimulation nonetheless alters the responses evoked by stimulation within the CRF. In the visual cortex, these nonclassical receptive field (nCRF) effects often contribute to the neural correlates of visual perceptual phenomena, such as illusory contours(von der Heydt et al., 1984, Ramsden et al., 2001), visual salience and boundary segmentation(Knierim and van Essen, 1992, Sillito et al., 1995, Yan et al., 2018, Lee et al., 2002, Nothdurft et al., 1999), contour integration(Nelson and Frost, 1985, Kapadia et al., 1995, Li et al., 2006), figure-ground segregation(Lamme, 1995, Zipser et al., 1996, Poort et al., 2012), and border ownership(Zhou et al., 2000, von der Heydt, 2015, von der Heydt, 2023).

In contrast to the feedforward mechanisms underlying the CRF, nCRF effects are thought to be generated either by feedback from neurons with larger CRFs in higher areas(Hupe et al., 1998, Bullier et al., 2001, Bair et al., 2003, Nassi et al., 2013, Chen et al., 2017, Klink et al., 2017, Zhang et al., 2014, Nurminen et al., 2018, Keller et al., 2020, Pak et al., 2020, Vangeneugden et

al., 2019, Gieselmann and Thiele, 2022, Chen et al., 2014, van Kerkoerle et al., 2014), or through intracortical horizontal connections(Adesnik et al., 2012, Chisum et al., 2003, Stettler et al., 2002), or by both(Angelucci and Bressloff, 2006, Schwabe et al., 2006, Ichida et al., 2007, Angelucci et al., 2017, Liang et al., 2017, Self et al., 2013). In contrast to feedforward inputs, feedback and horizontal inputs to V1 both avoid layer 4C and terminate predominantly in superficial and deep layers(Rockland and Lund, 1983, Rockland and Pandya, 1979, Rockland and Virga, 1989, Anderson and Martin, 2009, Markov et al., 2014, Federer et al., 2021, Gilbert and Wiesel, 1983, Shmuel et al., 2005). These differences between feedforward and feedback/horizontal circuitry suggest that the flow of signals across V1 layers should covary with the type of visual stimulation.

Newly developed, high-density Neuropixels probes have enabled recordings from a large, dense population of neurons(Jun et al., 2017, Trautmann et al., 2023), and dramatically increase the quantity of identifiable functional interactions between pairs of neurons, particularly in non-human primates(Trepka et al., 2022). Recently, this approach was used to recapitulate known circuit properties, such as the pairwise lead-lag relationship between simple and complex cells and the canonical laminar input-output relationship in macaque V1(Trepka et al., 2022), as well as the visual hierarchy in mouse visual cortical(Siegle et al., 2021, Jia et al., 2022) and subcortical areas(Sibille et al., 2022). Here, using Neuropixels probes, we recorded the activity of hundreds of neurons simultaneously from single V1 columns in the macaque brain during CRF and nCRF stimulation. We leveraged the high yields obtained from different layers to examine the organization and circuitry underlying contextual modulation.

Results

Classical RF stimulation in single V1 columns

Neuronal activity was recorded in two anesthetized rhesus macaques (M1 and M2, *Macaca Mulatta*) using high-density, multi-contact Neuropixels probes (version 3A, IMEC Inc., Belgium) (Figure 1A) (Methods). Neuropixels probes were inserted into the lateral operculum of V1 with the aid of a surgical microscope at angles nearly perpendicular to the cortical surface. Boundaries of laminar compartments were estimated by combining current-source density (CSD) measurements and histological data (Figure 1B; Figure S1) (Methods). Each recorded neuron was assigned to one of 4 laminar compartments, specifically 5/6, 4C, 4A/B, 2/3 (Mean thickness: 489, 281, 311, 650µm, respectively, consistent with previous anatomical(O'Kusky and Colonnier, 1982, Lund, 1973) and CSD(Self et al., 2013, Chen et al., 2017) studies). We measured the responses of a total of 677 and 621 visually driven neurons to classical and nonclassical receptive field (RF) stimulation, respectively (Methods), in 4 Neuropixels probe penetrations (2 in M1, *pen1-pen2*, ~4-6° eccentricities; 2 in M2, *pen3-pen4*, ~6-10° eccentricities). As a result of the nearly perpendicular penetrations, visual RFs of V1 neurons were largely overlapping across the cortical depth (Figure 1C).

During each recording session, neurons were first tested with classical RF (CRF) stimuli composed of drifting Gabor gratings of 1.5 degrees of visual angle (dva) in diameter, presented at the joint RF location of simultaneously recorded neurons (Methods). In each of the 4 recordings, neurons across cortical depth exhibited very similar preferences to grating orientations (Figure 1D). The modal pairwise difference in preferred orientation between all neurons across layers was near zero (*pen1*=5°; *pen2*=5°; *pen3*=1°; *pen4*=1°). This result confirmed that our recordings were nearly perpendicular and included neurons predominantly from single orientation columns.

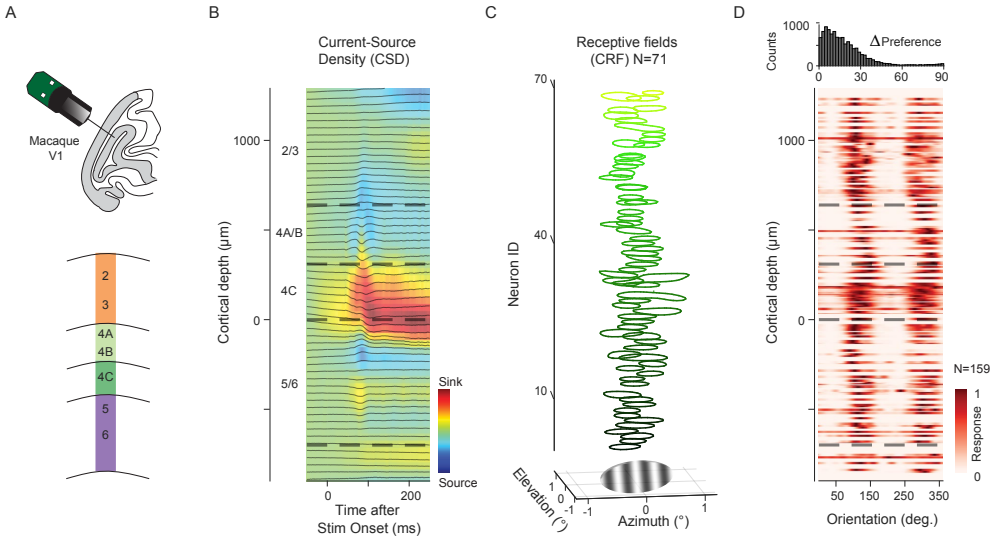

Figure 1. Classical receptive field (CRF) stimulation in single V1 columns.
(A). Neuropixels probe (384 channels/3.84mm) penetrations made into the lateral surface and underlying calcarine sulcus of macaque V1. Lower, diagram of designated laminar compartments. (B). Current-Source density (CSD) profile for one example recording session (M1, *pen1*) showing the early current sink (red) indicative of layer 4C. Laminar compartment boundaries (dashed lines) were determined using histological data and the CSD profile. (C). Top, 71 well-defined classical receptive fields (CRF) vertically stacked along the cortical depth. Bottom, drifting Gabor grating stimulus used for CRF stimulation. (D). Heat map of visual responses of 159 neurons to 36 drift directions of Gabor gratings shown vertically stacked along the cortical depth (M1, *pen1*). Top, distribution of differences in preferred orientation for all pairwise combinations of neurons.

Gratings were sized to largely restrict the stimuli within the CRFs of recorded neurons to maximize the extent to which V1 responses were driven in large proportion by feedforward circuitry. In V1, geniculocortical inputs initially drive neurons within layers 4Cα, 4Cβ, and layer 6(Hubel and Wiesel, 1972, Hendrickson et al., 1978, Blasdel and Lund, 1983), which then propagate to supragranular and infragranular layers(Callaway, 1998, Callaway, 2004).

Nonclassical RF stimulation and border ownership

Within each of the recordings, we also examined the responses of V1 neurons to nonclassical RF (nCRF) stimuli. It is known that neurons in primate visual cortex integrate visual information from

far beyond their CRFs(Albright and Stoner, 2002, Allman et al., 1985, Fitzpatrick, 2000, Roelfsema, 2006, Angelucci et al., 2017). One example of contextual modulation is the selectivity of neurons to border ownership (B_{own}). Specifically, neurons in early visual areas respond differently to identical edges (borders) of objects when those objects lie at different locations outside of the CRFs(Zhou et al., 2000, Franken and Reynolds, 2021, Hesse and Tsao, 2016, Hesse and Tsao, 2023) (Figure 2). As with other forms of nCRF modulation, B_{own} is thought to emerge either by feedback from higher areas(Craft et al., 2007, Jehee et al., 2007, Layton et al., 2012, Eguchi and Stringer, 2016, Wagatsuma et al., 2021, Mehrani and Tsotsos, 2021) or from horizontal connections within the same area(Zhaoping, 2005, Kogo et al., 2010). In V1, feedback and horizontal inputs arrive principally within supragranular and infragranular layers, i.e., they avoid layer 4(Rockland and Pandya, 1979, Rockland and Lund, 1983, Rockland and Virga, 1989, Anderson and Martin, 2009, Markov et al., 2014, Federer et al., 2021, Gilbert and Wiesel, 1983, Shmuel et al., 2005). Thus, V1 activity generated by nCRF stimulation is known to involve different circuits compared to the activity generated by CRF stimulation.

In this study, border ownership test stimuli consisted of uniformly white or black objects (squares, 8 x 8 dva) on a black or white background, respectively, as in previous studies(Zhou et al., 2000). One border of the object fell within the CRFs of the recorded neurons (Methods). Within the CRF, the oriented border could either be a dark-light edge or light-dark edge, resulting in two different local contrast polarity (LC) conditions (Figure 2A). Outside the CRF, the stimulus configuration differed for the same LC condition such that the oriented border could belong to opposite sides of an object relative to the CRF. Crucially, across these two object side conditions, the stimulus falling within the CRF was identical (Figure 2B) and was identical within an area that extended well beyond the CRF (8 x 16, dva). In this stimulus configuration, differences in evoked

responses between the two object side conditions signify selectivity to border ownership(Zhou et al., 2000).

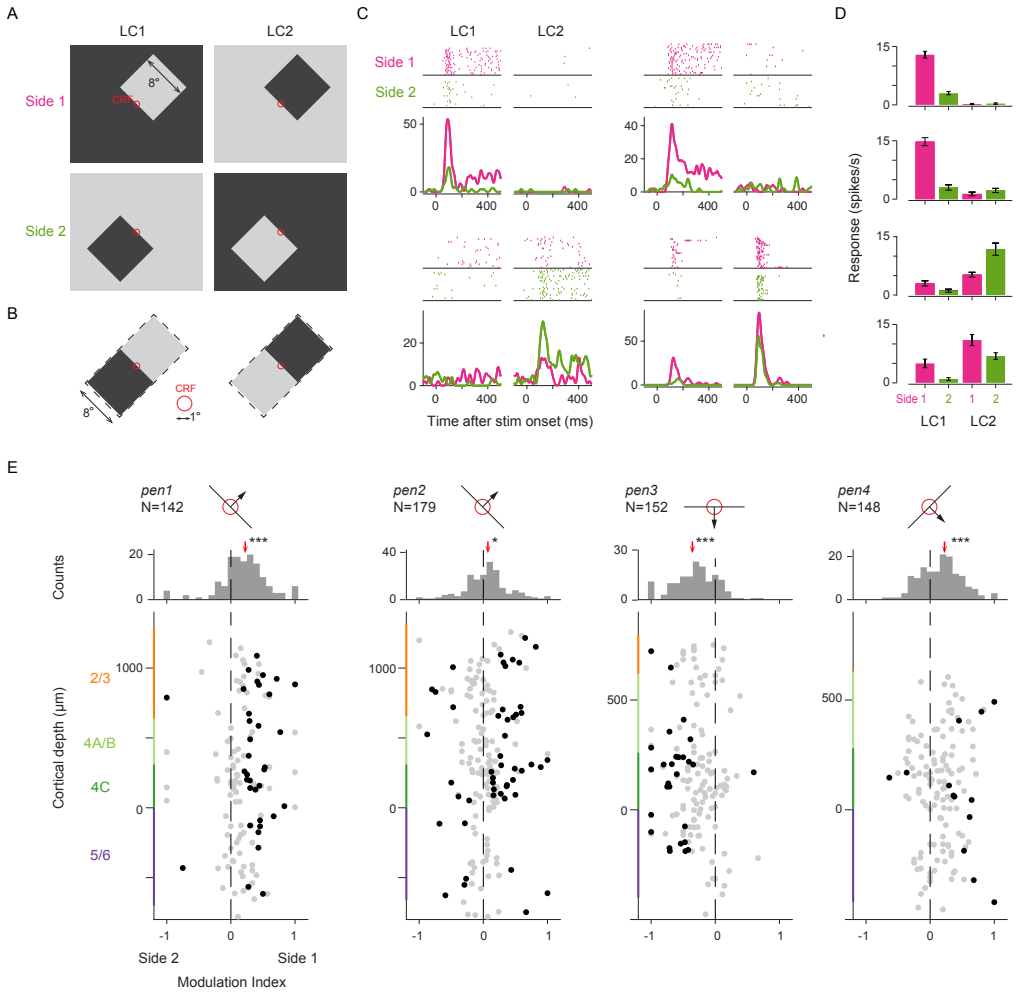

Figure 2. Nonclassical receptive field (nCRF) stimulation and border ownership.
(A). Border ownership test stimuli for nCRF stimulation. Stimuli consisted of uniformly white or black objects (8º squares) on a black or white background, respectively. One border of the object fell within the CRFs (red circle) of the recorded neurons at an orientation that varied in 45º steps. Within the CRF, depending on the local contrast polarity (LC), the oriented border could either be a dark-light edge (LC1, Left column) or a light-dark edge (LC2, Right column). For the same LC condition, the border within CRF could be the bottom-left edge (side 1, top row) or top-right edge (side 2, bottom row) of an object. (B). Enlarged view of stimulus configuration within CRF showing the identical stimulus regions between side 1 and side 2, for each LC condition (8 x 16, dva). (C). Four example B_{own} neurons recorded from V1. For each example neuron, plots of dot raster (top) and instantaneous firing rate (bottom) show responses to the 4 stimulus conditions depicted in (A), respectively. Magenta, side 1 condition; Green, side 2 condition. (D). Bar plots show mean spike rates of the 4 neurons across the 4 stimulus conditions. (E). Top, Cartoon depicts the preferred border orientation for each of 4 recording sessions (*pen*1-4). Arrow points to the

preferred side of objects relative to the border in the CRF. Bottom, side modulation index for each neuron plotted at its recorded cortical depth for each of the 4 recordings. Color bars on the y axis label the laminar compartment. Black colored dots denote statistically significant neurons for B_{own}. Middle, marginal distribution of the side modulation index. Red arrow indicates the population median. *$p<0.05$; ***$p<10^{-5}$.

We observed neurons with B_{own} in our recordings from macaque V1. Figure 2C and 2D shows examples of four neurons selective to border ownership. Each of the example neurons exhibited a preference for LC, with two neurons preferring one contrast polarity and two preferring the other. In addition, each neuron also responded differently depending on which side of the object appeared relative to the CRF, thus exhibiting B_{own}. Three of the neurons responded more vigorously to borders belonging to the lower-left side of object (side 1), and one neuron responded more vigorously to the border belonging to the upper-right side of the object (side 2). Furthermore, one of the neurons exhibited a preference for the same side of the object (side 1) for both LCs.

We recorded a total of 621 visually responsive V1 neurons across 4 recording sessions and measured their selectivity to border ownership (N=142; 179; 152; 148, in each recording, respectively). To quantify the B_{own}, as in previous studies(Zhou et al., 2000), we calculated a side modulation index, which is defined as the difference in neuronal responses to borders belonging to opposite sides of objects, divided by their sum (Methods). Responses to the same side of object, but opposite LC conditions, were averaged together to control for the global luminance differences in the overall display. Across recording sessions, we found that 133 neurons (21.4%) responded differently to identical borders yet belonging to opposite sides of the object ($p<0.05$, two-way ANOVA), a proportion consistent with previous studies(Zhou et al., 2000). Neurons with B_{own} were found within all cortical laminar compartments, including input layer 4C (5/6: 28/144=19.4%; 4C: 48/212=22.6%; 4A/B: 19/114=16.7%; 2/3: 28/99=28.3%), and the proportion was independent of laminar compartment ($\chi^2(3)=4.78$, $p=0.19$, chi-square test of homogeneity).

Of all V1 neurons, 96 (15.5%) exhibited B_{own} depending on the local contrast (5/6: 16/144=11.1%; 4C: 38/212=17.9%; 4A/B: 16/114=14.0%; 2/3: 20/99=20.2%), whereas 37 neurons (6.0%) showed significant effects independent of local contrast (5/6: 12/144=8.3%; 4C: 10/212=4.7%; 4A/B: 3/114=2.6%; 2/3: 8/99=8.1%). Thus, the majority of V1 neurons with B_{own} exhibited selectivity at only one local contrast, and neurons with B_{own} invariant to local contrast were rare, also consistent with previous observations(Zhou et al., 2000).

Columnar organization of border ownership selectivity

We next considered whether neurons with B_{own} comprised a distinct group, or instead reflected a general tendency of neurons to prefer one side of the object, with statistically significant neurons falling at the tails of the distribution. We leveraged the large number of simultaneously recorded single neurons to measure the distribution of side modulation across laminar compartments in each session. We found that in each of the four recordings, the distributions of side modulation generally appeared unimodal, with neurons exhibiting B_{own} falling at the distribution tails (Figure 2E). Surprisingly, we also found that within individual recordings, neurons across the cortical depth tended to share similar preferences for the side of the object. That is, for each recording, the side modulation differed significantly from 0 (Median modulation index: *pen1*= 0.20, $p<10^{-12}$; *pen2*= 0.06, p=0.04; *pen3*= -0.32, $p<10^{-15}$; *pen4*= 0.20, $p<10^{-5}$, sign test against zero-median). For example, the first recording (*pen1*) was performed in a column in which most neurons preferred an orientation of 135°. In addition, within that column, neurons tended to exhibit higher responses to a border when it belonged to the lower-left side of an object (side 1), as opposed to the upper-right side (side 2). Thus, V1 exhibited a continuum of B_{own}, and neurons within single columns tended to prefer the same side of objects located outside of the CRF.

Functional interactions among neurons within single V1 columns

The large number of simultaneously recorded neurons from each session also allowed us to measure functional interactions among single neurons under different visual stimulation conditions. Temporally precise cross-correlations in spike trains offer a unique means of assessing functional interactions among neurons in neural circuits(Perkel et al., 1967). Cross-correlations can be interpreted as suggesting one of myriad putative circuit arrangements among neuronal ensembles(Moore et al., 1970, Aertsen and Gerstein, 1985, Melssen and Epping, 1987, Ostojic et al., 2009). The identification of such interactions has played an important role in elucidating neural circuits in the mammalian visual system(Ts'o et al., 1986, Schwarz and Bolz, 1991, Reid and Alonso, 1995, Alonso et al., 1996, Alonso and Martinez, 1998, Usrey et al., 1998, Nelson et al., 1992, Briggs et al., 2013, Roe and Ts'o, 1999, Senzai et al., 2019, Denman and Contreras, 2014, Siegle et al., 2021, Jia et al., 2022, Trepka et al., 2022, Smith and Kohn, 2008, Sibille et al., 2022). In particular, it has been useful in specifying the flow of signals through local neural circuits(Trepka et al., 2022) and distributed networks(Siegle et al., 2021, Jia et al., 2022, Sibille et al., 2022). Notably, past studies have demonstrated that neuronal cross-correlations are dynamic and can depend on stimulus context and behavioral variables(Hembrook-Short et al., 2019, Martin and von der Heydt, 2015, Hung et al., 2007, Hirabayashi and Miyashita, 2005, Hirabayashi et al., 2010, Steinmetz et al., 2000).

Given that V1 activity generated by nCRF stimulation is thought to involve different circuitry than activity generated by CRF stimulation(Angelucci et al., 2017), we next asked if the pattern of functional interactions measured under classical and nonclassical stimulus conditions might differ in a manner consistent with models of their underlying circuitry. Specifically, modulation of visual responses during nCRF stimulation, such as border ownership stimuli, is

thought to emerge from either feedback from higher areas or horizontal connections within the same areas(Bair et al., 2003, Bullier et al., 2001, Hupe et al., 1998, Chen et al., 2017, Gieselmann and Thiele, 2022, Keller et al., 2020, Klink et al., 2017, Nassi et al., 2013, Nurminen et al., 2018, Angelucci et al., 2017, Angelucci and Bressloff, 2006, Ichida et al., 2007, Schwabe et al., 2006, Pak et al., 2020, Vangeneugden et al., 2019, Zhang et al., 2014, Adesnik et al., 2012, Chisum et al., 2003, Stettler et al., 2002, Liang et al., 2017, Craft et al., 2007, Jehee et al., 2007, Chen et al., 2014, Self et al., 2013, van Kerkoerle et al., 2014), both arriving principally in superficial and deep layers(Rockland and Lund, 1983, Rockland and Pandya, 1979, Rockland and Virga, 1989, Markov et al., 2014, Federer et al., 2021, Anderson and Martin, 2009, Gilbert and Wiesel, 1983, Shmuel et al., 2005). In contrast, CRF responses are driven predominantly by feedforward circuitry and geniculocortical inputs to layers 4C and 6(Hubel and Wiesel, 1972, Hendrickson et al., 1978, Blasdel and Lund, 1983, Callaway, 1998, Callaway, 2004). This suggests that the functional interactions among neurons across V1 layers may differ under CRF and nCRF stimulus conditions.

Across recording sessions, we calculated cross-correlograms (CCGs) from all possible pairwise combinations of neuronal spike trains during both CRF (Gabor gratings) and nCRF (border ownership) stimulation conditions. Figure 3A shows an example recording session (M1, *pen1*) in which 159 visually responsive neurons were recorded during CRF stimulation, and CCGs were computed for all 12,561 pairwise combinations of neurons. CCGs were determined to be significant if the jitter-corrected CCG peak occurred within 10ms of zero-time lag, and if that peak was >7 standard deviations (SD) above the mean of the noise distribution(Siegle et al., 2021, Trepka et al., 2022) (Methods). Of the total CCGs computed in this recording, 13.8% were found to be significant. Eight significant pairs are highlighted in Figure 3A, and their corresponding CCGs are shown in Figure 3B. The peak lag (PL), defined as the relative time delay of the

occurrence of peak correlation between two spike trains, approximates the synchrony and/or the direction of functional interactions between neuronal pairs(Aertsen and Gerstein, 1985, Moore et al., 1970, Melssen and Epping, 1987, Ostojic et al., 2009). These examples illustrate the tendency of CCGs to corroborate the circuitry within V1 columns under CRF conditions in that 1) PLs generally increase with larger distances between pairs, and 2) layer 4 neurons tend to lead superficial neurons(Trepka et al., 2022). We exploited this latter point to test the extent to which the sequence of information flow across layers differs between CRF and nCRF conditions.

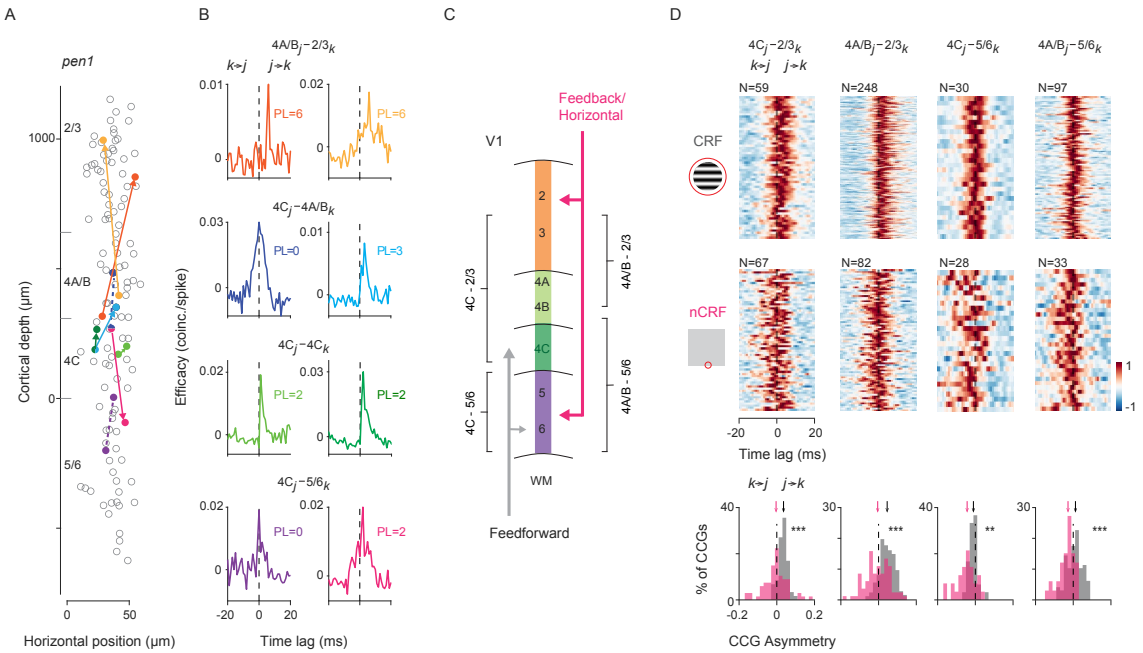

Figure 3. Interlaminar functional interactions during CRF and nCRF stimulation. (A). Example recording (M1, *pen1*) with 159 visually responsive neurons (circles) recorded simultaneously during CRF stimulation and plotted at their relative cortical depth. Horizontal axis is magnified for visualization. Shown also are eight example neuronal pairs with significant CCGs during CRF stimulation. Neuronal pairs with zero-time lag CCGs are connected with dashed lines. Pairs with nonzero-time lag CCGs are connected with arrowed lines. Arrow direction points to the lagging neuron. (B). Eight corresponding CCGs as shown in (A). Neuronal pairs are separated by their laminar compartment locations. The reference neuron (1st neuron in the CCG function) is designated as *j*; the target neuron is designated as *k*. PL: peak lag. (C). Diagram illustrating feedforward and feedback (and horizontal) projections within the designated laminar compartments. Feedforward inputs arrive within laminar compartments 4C and 6, whereas feedback (and horizontal) projections principally target superficial and deep layers. (D). Heat map of all significant CCGs during either CRF stimulation (Gabor gratings, top row) or nCRF stimulation (border ownership, middle row), for the 4 key interlaminar combinations (four

columns), calculated from one example recording (M1, *pen1*). Individual CCGs are normalized by their absolute maximum values for visualization, different CCGs are vertically stacked. Bottom row, distribution of CCG asymmetry for each of the 4 key interlaminar compartments as in (A), across CRF stimulation condition (gray) and nCRF stimulation condition (magenta). Arrows indicate the population median. **$p<0.002$; ***$p<10^{-5}$.

Comparison of functional interactions during CRF and nCRF stimulation.

From the 677 and 621 neurons recorded across the 4 recording sessions during CRF and nCRF stimulation, there were 41,759 and 28,430 pairwise combinations included, respectively (Methods). Of those, we found that 6,937 (16.6%) and 4,826 (17.0%) of the CCGs were significant. Notably, the rates were nearly identical under the two stimulus conditions, and also were within the range observed in previous studies of macaque V1(Chu et al., 2014, Hembrook-Short et al., 2019, Smith and Kohn, 2008, Kohn and Smith, 2005).

As noted above, modulation of visual responses during nCRF stimulation, such as border ownership stimuli, is thought to be generated principally by feedback/horizontal connections arriving within superficial and deep layers, which contrasts with feedforward input driving CRF stimulation (Figure 3C). Thus, we asked whether the functional interactions of pairs of neurons situated across laminar compartments depended on the type of visual stimulation. We focused our analysis on CCGs computed from pairs of neurons in which one neuron was located within laminar compartments receiving feedback/horizontal inputs (FH_i) and the other was located within compartments largely devoid of those inputs, namely 4C and 4A/B. This analysis compared the interlaminar spike correlations between neuronal pairs during CRF and nCRF stimulation. If indeed FH_i contribute more to activity during the latter than the former, then we should expect this to be reflected in lead-lag relationships of the CCGs.

A comparison of V1 CCGs between key interlaminar neuronal pairs during CRF and nCRF stimulation is shown for an example recording session (M1, *pen1*) in Figure 3D. During CRF

stimulation, the timing of spikes within compartments 4C and 4A/B generally preceded, or was simultaneous with, spikes within FH_i compartments (CRF: 4C-2/3$_{PL}$=2ms, $p<10^{-7}$; 4A/B-2/3$_{PL}$=2ms, $p<10^{-28}$; 4C-5/6$_{PL}$=0ms, p=0.52; 4A/B-5/6$_{PL}$=0ms, p=0.64; Sign test against zero-median). In contrast, during nCRF stimulation, the sequence of spike timing was shifted in favor of neurons in FH_i compartments. Specifically, during nCRF stimulation, the timing of spikes within compartments 4C and 4A/B lagged or was simultaneous with, spikes within FH_i compartments (nCRF: 4C-2/3$_{PL}$=0ms, p=0.80; 4A/B-2/3$_{PL}$=0ms, p=0.70; 4C-5/6$_{PL}$=-2.5ms, p=0.11; 4A/B-5/6$_{PL}$=0ms, p=0.56; Sign test against zero median). To further quantify the apparent shift in lead-lag relationships, we calculated an asymmetry index for each CCG. The asymmetry index is computed as the difference in the CCG integral on either side of zero-time lag, and summarizes the lead-lag relationship independent of the CCG peak(Jia et al., 2022) (Methods). Consistent with the analyses of PL, we found that CCG asymmetries differed significantly between CRF and nCRF stimulation for each of the interlaminar comparisons. In each case, the distribution of asymmetries during nCRF stimulation shifted to favor neurons in FH_i laminar compartments, when compared to CRF stimulation (4C-2/3: CRF_{Asym}=0.036, $nCRF_{Asym}$=-0.004, Δ=-0.04, $p<10^{-6}$; 4A/B-2/3: CRF_{Asym}=0.046, $nCRF_{Asym}$=-0.005, Δ=-0.051, $p<10^{-11}$; 4C-5/6: CRF_{Asym}=-0.010, $nCRF_{Asym}$=-0.044, Δ=-0.034, p=0.0015; 4A/B-5/6: CRF_{Asym}=0.012, $nCRF_{Asym}$=-0.028, Δ=-0.04, $p<10^{-5}$; Wilcoxon rank-sum test). Thus, data from this single recording session indicated that interlaminar spike timing was earlier within FH_i laminar compartments during nCRF stimulation than during CRF stimulation.

Across all recordings, we identified a total of 2,573 and 2,118 significant neuronal pairs from the four interlaminar combinations during CRF or nCRF stimulation, respectively, and compared their CCG asymmetries. Similar to the pattern observed in the example recording, we

observed a consistent shift in lead-lag relationships for each of the interlaminar comparisons (Figure 4A). Specifically, during nCRF stimulation, the distribution of asymmetries during nCRF stimulation shifted to favor neurons in FH_i laminar compartments, when compared to CRF stimulation (4C-2/3: CRF_{Asym}=0.028, $nCRF_{Asym}$=0.012, Δ=-0.016, $p<10^{-9}$; 4A/B-2/3: CRF_{Asym}=0.038, $nCRF_{Asym}$=0.022, Δ=-0.016, $p<10^{-9}$; 4C-5/6: CRF_{Asym}=-0.033, $nCRF_{Asym}$=-0.047, Δ=-0.014, $p<10^{-5}$; 4A/B-5/6: CRF_{Asym}=-0.018, $nCRF_{Asym}$=-0.05, Δ=-0.032, $p<10^{-20}$; Wilcoxon rank-sum test). Thus, the interlaminar spike timing was earlier within FH_i laminar compartments during nCRF stimulation than during CRF stimulation in the combined dataset. Notably, we observed a similar pattern of results when instead of asymmetry, we compared CCG peak lags (Figure S2A), and when we compared the total number of significant and nonsignificant pairs (CRF = 15,920; nCRF = 11,263) (Figure S2B), and when we compared CCGs with a more stringent significance criterion (10 SDs) in the combined dataset (Figure S2C-D).

Lastly, we asked whether differences in interlaminar cross-correlations between CRF and nCRF stimulation were related specifically to border ownership, as opposed to other differences in the two types of stimuli (e.g., size). We considered that if the relative timing of spiking activity within FH_i laminar compartments is indicative of nCRF modulation, then there should be a relationship between that timing and the magnitude of modulation, i.e., B_{own}. That is, we should expect earlier relative spike timing in FH_i laminar compartments, i.e., lower CCG asymmetries with respect to other compartments, to be associated with greater B_{own} in the constituent neuronal pairs. To test this, we built a generalized linear model (GLM) to measure the relationship between

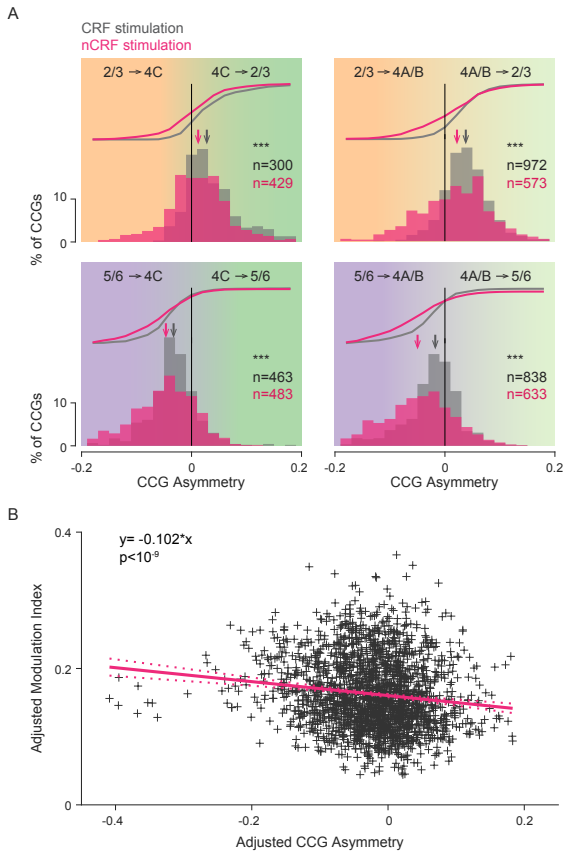

Figure 4. Shift in relative spiking time across sessions and its effect on nCRF modulation. (A). Combined dataset for each of the 4 key interlaminar combinations. Histograms and cumulative distributions of asymmetry for all significant CCGs during CRF (gray) and nCRF (magenta) stimulation. Arrows indicate the population median. ***$p<10^{-5}$. (B). Scatter plot of B_{own} modulation index against CCG asymmetry for all significant CCGs aggregated over the 4 interlaminar combinations. Values are adjusted by a GLM to partial out variance from different laminar combinations. Solid magenta line denotes the fitted dependence in the GLM, and the dashed lines denote the 95% confidence interval.

CCG asymmetry and B_{own} across all significant neuronal pairs and all four interlaminar combinations. In the GLM, we used the CCG asymmetry of each neuronal pair and the four interlaminar combinations as factors to explain the B_{own}; the latter was calculated as the geometric mean B_{own} of the neuronal pair (Methods). Indeed, we found that lower CCG asymmetries, i.e., earlier spike timing in FH_i laminar compartments relative to other compartments, were predictive of larger values of B_{own} across the laminar combinations (Slope = -0.10, $p<10^{-9}$) (Figure 4B) (Table

S1). This result indicates that contextual modulation via nCRF mechanisms was associated with greater information flow from FH_i laminar compartments.

Discussion

We measured the sensitivity of neurons to nCRF stimulation, specifically border ownership, within large, local populations in macaque V1. Consistent with previous studies, we observed V1 neurons with border ownership selectivity. We observed that neurons within single columns tended to prefer the same side of objects located outside of the CRF. In addition, we found that the functional interactions among pairs of neurons situated across FH_i and other laminar compartments differed between CRF and nCRF stimulation. Specifically, neurons within FH_i laminar compartments were more likely to lead pairwise interactions with neurons in other compartments during nCRF stimulation than during CRF stimulation. Moreover, the magnitude of border ownership modulation was predicted by greater information flow from FH_i laminar compartments. These results demonstrate that the flow of signals between neurons in FH_i and other laminar compartments depends on the degree to which those neurons integrate visual information from beyond the classical receptive field. Below we discuss some potential limitations of the results as well as their implications for the mechanisms underlying contextual modulation.

Each of the laminar compartments designated in this study comprised more than a single distinct anatomical layer. This was done to mitigate the uncertainty in determining exact laminar boundaries, to achieve comparable numbers of neurons across compartments, and to maximize statistical power. In addition, combining layers allowed us to combine feedback with horizontal input layers. It is known that feedback and horizontal connections exhibit layer specificity within superficial and deep layers, e.g., horizontal connections are most prominent in layer 2/3 and layer 5(Rockland and Lund, 1983, Gilbert and Wiesel, 1983), where feedback connections target primarily in layers 1, upper layer 2, and 5/6(Rockland and Pandya, 1979, Federer et al., 2021, Shmuel et al., 2005). Yet, they both largely avoid layer 4(Angelucci et al., 2017). Nonetheless,

given that the number of anatomically distinct layers within macaque V1 well exceeds the four designated laminar compartments used here, it is important to consider the extent to which collapsing layers limits the conclusions one can draw from our observations. For example, although layer 6 receives feedback input, it also receives feedforward input directly from the LGN(Hubel and Wiesel, 1972, Hendrickson et al., 1978, Blasdel and Lund, 1983, Callaway, 1998). In addition, layer 4A is generally considered an input layer whereas 4B is not(Callaway, 1998, Hubel and Wiesel, 1972, Blasdel and Lund, 1983, Hendrickson et al., 1978). Thus, the designation of any compartment as nominally input, or feedback was relative and not absolute. That is, superficial and deep layers receive higher proportions of feedback/horizontal inputs than the 4A/B and 4C compartments. Indeed, previous studies of primate visual cortex have used a similar approach in comparing input and feedback/horizontal laminar compartments, e.g.,(Hansen et al., 2012, Nandy et al., 2017, van Kerkoerle et al., 2017, Pettine et al., 2019). Thus, the observed changes in functional interactions between neurons situated across compartments with different relative feedforward and feedback/horizontal input can be interpreted in light of those input differences.

Another important consideration is that a key challenge of studying classical and nonclassical RF effects simultaneously in large neuronal populations is the difficulty in achieving alignment of all CRFs with the test stimuli. Although our electrode penetrations were largely normal to the surface and neurons showed minimal deviations in orientation selectivity across the cortical depth, V1 neurons nonetheless exhibit noteworthy RF scatter (location/size) even within single cortical columns(Tootell et al., 1988, Gur et al., 2005, Li et al., 2022). This means that the positioning of stimuli relative to the CRF inevitably varied across simultaneously recorded neurons (e.g., Figure 1C). Moreover, this means that although neurons were generally well driven by CRF

grating stimuli and exhibited clear orientation tuning, CRF stimulation was not guaranteed to fall solely within the CRF of all neurons. Nonetheless, involvement of the surround, especially far surround was considerably less extensive for CRF stimulation than for nCRF stimulation. Furthermore, in the latter case, regardless of variability in the CRF location, stimuli falling within the CRF were always matched across nCRF stimulus conditions, and the surrounds were also identical within 8° of the CRF (Figure 2A, B).

The experiments described here were performed in anesthetized animals. Notably, many previous studies have also described contextual modulation in anesthetized animals using a variety of different nCRF stimulation(Ramsden et al., 2001, Hupe et al., 1998, Bair et al., 2003, Allman et al., 1985, Gilbert and Wiesel, 1990, Nothdurft et al., 1999, Webb et al., 2003, Zarella and Ts'o, 2016, Muller et al., 2003, Henry et al., 2013). Nonetheless, anesthesia is known to affect at least some forms of contextual responses in areas V1, for example figure-ground segregation(Lamme et al., 1998), which presumably relies on attention, object recognition and saccade planning(Super et al., 2001, Poort et al., 2012). However, border ownership modulation can act separately even without attention(Qiu et al., 2007) or before object shape recognition(Williford and von der Heydt, 2016), perhaps signifying a representation of “proto-objects” in the early visual cortex through pre-attentive grouping mechanism(von der Heydt, 2015, von der Heydt, 2023, Self et al., 2019). Thus, border ownership and other types of contextual modulation may be less affected by anesthesia despite a dependence on cortical feedback.

Border ownership enables neurons with small CRFs in the early visual cortex to assign the occluding border between image regions to a foreground object, which is crucial for natural scene segmentation and object recognition(Nakayama et al., 1995). Human imaging studies have demonstrated the existence of B_{own} in both lower(Fang et al., 2009) and higher visual areas(Kourtzi

and Kanwisher, 2001, Andrews et al., 2002), yet the underlying circuitry is still poorly understood. Several computational models have been proposed to explain B_{own}, including feedforward models(Walker et al., 1999, Sakai and Nishimura, 2006, Super et al., 2010), horizontal models(Zhaoping, 2005, Kogo et al., 2010), and feedback models(Craft et al., 2007, Jehee et al., 2007, Jeurissen et al., 2016). Yet cues for determining B_{own} often lie far from the CRF, and only feedback connections are well suited to mediate contextual modulation from far regions of the surround(Angelucci et al., 2017). Besides, conduction along horizontal fibers appears too slow (0.1~0.4 mm/msec)(Grinvald et al., 1994, Bringuier et al., 1999, Girard et al., 2001) to account for the fast (~20ms) emergence of B_{own}. And the onset of B_{own} modulation is independent of the object size(Zhang and von der Heydt, 2010, Sugihara et al., 2011). Feedback fibers could conduct 10 times faster (20-60 mm/msec) than horizontal connections(Girard et al., 2001) and could contribute to modulating the early responses of V1 neurons(Hupe et al., 2001, Bair et al., 2003, Nassi et al., 2013). Thus, although we combined feedback and horizontal recipient layers, the differences in interlaminar signal flow we observed were likely driven predominantly by feedback inputs.

In primates, V1 receives interareal feedback connections primarily from areas V2, V3, V4, MT(Rockland et al., 1994, Markov et al., 2014). Thus, V1 B_{own} signals could be generated via inputs from these areas(Zhou et al., 2000, Hesse and Tsao, 2016, Hesse and Tsao, 2023, Franken and Reynolds, 2021, Zhu et al., 2020). Our results resonate with a recent study reporting that in area V4, B_{own} emerges earliest in deep layers compared to input layers(Franken and Reynolds, 2021). This suggests that the earliest component of B_{own} in V4 is not inherited from feedforward inputs, i.e., from V1/V2, but is generated within deep layers de nova, or through feedback connections that arrive at deep layers(Franken and Reynolds, 2021). This further supports the view

that B_{own} in V1 emerges via feedback from higher visual areas. In addition, similar to what we observed in V1, columnar organization of B_{own} was observed in V4(Franken and Reynolds, 2021). Indeed, neurons with B_{own} are clustered into patches in a wide range of primate visual areas, including area V2, V3, V3A, V4, V4A(Hesse and Tsao, 2023). Thus, the evidence of B_{own} modularity we observed in V1 could arise from organized feedback from the B_{own} modules in those areas. This is supported by recent anatomical evidence suggesting that feedback terminals in V1 are clustered and functionally specific(Angelucci et al., 2002, Federer et al., 2021, Shmuel et al., 2005).

Methods

Subjects

Recordings were conducted in 2 anesthetized adult male rhesus macaques (*Macaca Mulatta*, M1, 13 kg; M2, 8 kg). The number of animals used is typical for primate neurophysiological experiments. All experimental procedures were in accordance with National Institutes of Health Guide for the Care and Use of Laboratory Animals, the Society for Neuroscience Guidelines and Policies, and with approved Institutional Animal Care and Use Committee (IACUC) protocol (#APLAC-9900) of Stanford University.

Electrophysiological Recordings

Prior to each recording session, treatment with dexamethasone phosphate (2 mg per 24 h) was instituted 24 h to reduce cerebral edema. After administration of ketamine HCl (10 mg per kilogram body weight, intramuscularly), monkeys were ventilated with 0.5% isoflurane in a 1:1 mixture of N_2O and O_2 to maintain general anesthesia. Electrocardiogram, respiratory rate, body temperature, blood oxygenation, end-tidal CO_2, urine output and inspired/expired concentrations of anesthetic gasses were monitored continuously. Normal saline was given intravenously at a variable rate to maintain adequate urine output. After a cycloplegic agent was administered, the eyes were focused with contact lenses on a CRT monitor. Vecuronium bromide (60 µg/kg/h) was infused to prevent eye movements.

With the anesthetized monkey in the stereotaxic frame, an occipital craniotomy was performed over the opercular surface of V1. The dura was reflected to expose a small (~3 mm^2) patch of cortex. Next, a region relatively devoid of large surface vessels was selected for implantation, and the Neuropixels probe was inserted with the aid of a surgical microscope. Given

the width of the probe (70 µm x 20 µm), insertion of it into the cortex sometimes required multiple attempts if it flexed upon contacting the pia. The junction of the probe tip and the pia could be visualized via the (Zeiss) surgical scope, and the relaxation of pia dimpling was used to indicate penetration, after which the probe was lowered at least 3-4 mm. Prior to probe insertion, it was dipped in a solution of the DiI derivative FM1-43FX (Molecular Probes, Inc) for subsequent histological visualization of the electrode track.

Given the length of the probe (1 cm), and the complete distribution of electrode contacts throughout its length, recordings could be made either in the opercular surface cortex (M1) or within the underlying calcarine sulcus (M2), by selecting a subset of contiguous set of active contacts (n = 384) from the total number (n=986). Recordings were made at 1 to 2 sites in one hemisphere of each monkey. At the end of the experiment, monkeys were euthanized with pentobarbital (150 mg/kg) and perfused with normal saline followed by 1 liter of 1% (wt/vol) paraformaldehyde in 0.1 M phosphate buffer, pH 7.4.

Visual Stimulation

Visual stimuli were presented at manually mapped receptive fields (RFs) locations for each recording session on an LCD monitor (Model NEC-4010, Dimensions= 88.5cm (H) x 49.7cm (V), pixels= 1360 x 768, frame rate= 60 Hz) positioned 114 cm from the monkeys. RF eccentricities were ~ 4-6° (M1) and ~ 6-10° (M2). Visual stimuli were generated with customized MATLAB script, using the Psychophysics Toolbox extensions (version PTB-3)(Kleiner et al., 2007). A photodiode was used for measuring stimulus timing.

Classical receptive field (CRF) Stimuli consisted of drifting Gabor gratings of 1.5 dva in diameter and 100% Michelson luminance contrast. Gratings were centered at the manually

determined CRFs locations. Gratings drifted in 36 different directions between 0 to 360° in 10° steps in a pseudorandom order, with a speed of 2 degree/sec. Four spatial frequencies (0.5, 1, 2, 4 cycle/degree) were tested and the optimal SF for each recording session was selected offline to determine the orientation tunings of the recorded neurons. Each grating was presented for 1 second. A blank screen with equal luminance to the Gabor patch was presented for 0.25s during the inter-stimulus interval. Each condition was repeated 5 or 10 times.

Nonclassical receptive field (nCRF) stimuli used in this study, i.e., Border ownership test stimuli consisted of uniformly white or black objects (square, 8 x 8 dva) presented on a black or white background, respectively, like previous studies(Zhou et al., 2000). One border of the object fell within the CRFs of the recorded neurons at an orientation that varied in 45º steps. Objects were either 4 x 4 dva or 8 x 8 dva in size, and only conditions with 8 x 8 dva were selected for quantifying border ownership selectivity to tolerate the variation in the CRF locations. Stimuli were presented monocularly. For each of the 4 orientation conditions, there were 4 different basic conditions (Figure 2A). Within the CRF, the oriented border could either be a dark-light edge or light-dark edge, resulting in two different local contrast (LC) polarity conditions, namely LC1 and LC2. For the same LC condition, the stimulus configuration outside of the CRF differed such that the oriented border could belong opposite sides of objects, resulting in two different side of object conditions, namely side 1 and side 2. Each object was presented for 1 second. A blank screen with equal luminance to the mean of object and background luminance was presented for 0.5s during the inter-stimulus interval. Each condition was repeated 10 or 20 times.

Data acquisition and spike sorting

Raw spike-band data was sampled and recorded at 30kHz. It was then median-subtracted and high-pass filtered at 300 Hz during the pre-processing stage. Spike-sorting was carried out with Kilosort3 *(https://github.com/MouseLand/Kilosort)* to find spike times and assign each spike to different templates (neurons). Default parameters in Kilosort3 were used for spike sorting, specifically, Ops.th=[9,9]; Ops.lam=20; Ops.AUCsplit=0.8; Ops.ThPre=8; Ops.sig=20; Ops.nblocks=5; Ops.spkTh=-6. The raw sorted data was then manually curated in Phy (*https://github.com/cortex-lab/phy*) to remove templates with very few spikes or with atypical waveforms and to perform minimal templates merging and splitting. Double counted spikes from algorithm fitting the residuals to a new template were identified using established criteria(Siegle et al., 2021), by counting spikes from two templates separated by less than 50μm (~5 channels) and with spike activity occurring within 5 samples (0.167ms). Double counted spikes from the template smaller in amplitude were removed from further analysis. Visual responsiveness of each unit was assessed under either CRF, nCRF, or RF mapping stimulation. For each type of stimulation, a paired-sample t test was performed to determine whether the mean spike counts after each stimulus presentation exceeded the preceding blank period at a significance level of 0.01. Only neurons show significant visual responsiveness were included for further analysis.

Layer Assignment

The laminar locations of our recorded neurons were estimated based on a combination of functional analysis and histology results. For each recording, we first performed the current source density (CSD) analysis on the stimulus-triggered average of local field potentials (LFP). LFP were low-pass filtered at 200 Hz and recorded at 2500 Hz. LFP signals recorded from every 4 nearby

channels were averaged and realigned to the onset of visual stimulus. CSD was estimated as the second-order derivatives of signals along the probe axis using the common five-point formula(Nicholson and Freeman, 1975). The result was then smoothed across space (σ = 120 μm) to reduce the artifacts caused by varied electrode impedance. We located the lower boundary of the major sink (the reversal point of sink and source) as the border between layer 4C and layer 5/6. Based on this anchor point, we assign other laminar compartment borders based on the thickness of the laminar compartments derived from DiI stained histological slices (Figure S1).

Receptive field mapping

In some sessions, the receptive fields of V1 neurons were tested systemically for offline use purpose. We measured CRFs by randomly presenting a single-probe stimulus out of a 10 x 10 probe grid extending 4 x 4 dva. The grid center was selected at the manually determined online RF center location. The probes consisted of circular sine wave grating of 0.4 dva in diameter, and 100% Michelson luminance contrast. Gratings were presented at the optimal orientation determined manually online for each recording session and drifted at speed of 2 degree/sec. Each grating was presented for 0.2s and interleaved with 0.3s of blank screen with equal luminance. Each location was repeated 15 times.

Mean spike counts from 0.05 to 0.25sec after each stimulus onset were calculated, resulting in a 10 x 10 matrix containing mean spike rates to each grid location. This 2D matrix was then interpolated to a 40 x 40 matrix (MATLAB function “interp2”) and then smoothed with a 2D gaussian filter (MATLAB function “imgaussfilt”, σ=2). The outline of the CRF was defined as the contour isoline at 80% of the maximum response using MATLAB function “contour3”. Neurons with only 1 contour region at the threshold were selected.

Single neuron properties during CRF stimulation

To assess the orientation tuning for each neuron, the spike rates during 0.1 to 1sec after each stimulus onset were calculated and averaged for each orientation condition (N=18). The orientation tuning responses were first smoothed with a Hanning window (half width at half height of 20°), and then fitted with a von-Mises function(Swindale, 1998)

$$y = a_0 + a_1 * e^{a_2*(\cos(2*x-2*a_3)-1)}$$

The location of the peak of the fitted curve was determined as the preferred orientation. Only neurons that were well fit by the function (R^2>0.7) were included. The pairwise differences in preferred orientation were then calculated for all the combinations for each recording session.

Modulation index for border ownership

As in previous studies(Zhou et al., 2000), we calculated a B_{own} modulation index to quantify the border ownership for each neuron, which is defined as

$$B_{own}\ modulation\ index = \frac{(R_{side1,lc1} + R_{side1,lc2}) - (R_{side2,lc1} + R_{side2,lc2})}{(R_{side1,lc1} + R_{side1,lc2}) + (R_{side2,lc1} + R_{side2,lc2})}$$

Where $R_{side(i),\ lc(i)}$ represents the average spike rate from 0.05 to 0.5sec after stimulus onset for one of 4 different basic conditions belonging to either side1 or side2, local contrast 1 (LC1) or local contrast 2 (LC2). The statistical significance of B_{own} was evaluated by performing a two-factor ANOVA (MATLAB function "anovan") on the average spike rate for each condition, the factors being object sides (two levels: side 1 and side 2) and local contrast (2 levels, LC1 and LC2), and the interaction term was also included. A significance level of 0.05 was chosen. Neurons were determined to exhibit significant B_{own} if they show significance in either the main effect or interaction for factor of object side.

Cross-correlograms (CCGs)

To measure correlated firing, we computed the crosscorrelation between spike trains of all pairs of simultaneously recorded neurons. Across recording sessions, we calculated cross-correlograms (CCGs) from all possible pairwise combinations of neuronal spike trains during either CRF (Gabor gratings) or nCRF (border ownership) stimulation conditions, respectively. For both conditions, we focused on the spiking activity within the 0.25 -1sec window during each stimulus presentation, to mitigate the influence of the transient visual response after stimulus onset. The CCG function for a given pair of neurons was defined as follows:

$$CCG(\tau)_{j-k} = \frac{\frac{1}{M}\sum_{i=1}^{M}\sum_{t=1}^{N-\tau} x_j^i\,(t) \times x_k^i(t+\tau)}{\theta(\tau)\sqrt{\lambda_j\lambda_k}}$$

where j denotes the first/reference neuron and k denotes the second/target neuron in the CCG function. τ is the time lag between the two spike trains x_j^i and x_k^i from neuron j and k, during trial i. The value of $x_j^i(t)$ and $x_k^i(t)$ is 1 if there is a spike at time bin t and is zero otherwise. M is the total number of trials; N is the number of time bins within a trial. $\theta(\tau) = N - |\tau|$, is a triangular function that corrects for the degree of overlap in the two spike trains at each time lag. λ_j and λ_k are the mean firing rates of neuron j and k computed over the same bins used to compute the CCG at each time lag. The normalization by the geometric mean of spike rates is commonly used by previous studies to account for the influence of firing rates on the CCG peaks(Bair et al., 2001, Kohn and Smith, 2005).

To correct for correlations due to stimulus-locking or slow fluctuations in the population responses (e.g., gamma-band activity), we computed a jitter-corrected CCG by subtracting a jittered CCG from the original CCG:

$$CCG_{corrected} = CCG_{original} - CCG_{jittered}$$

The jittered CCG ($CCG_{jittered}$) reflects the expected value of CCG computed from all possible jitters of each spike train within a given jitter window(Harrison and Geman, 2009, Smith and Kohn, 2008). The jittered spike train preserves both the PSTH of the original spike train across trials and the spike counts in the jitter window within each trial. As a result, jitter correction removes the correlation between PSTHs (stimulus-locking) and correlation on timescales longer than the jitter window (slow population correlations). Here, a 25-ms jitter window was chosen based on previous studies(Jia et al., 2013, Siegle et al., 2021). Jitter-corrected CCG ($CCG_{corrected}$) was then smoothed with a 5ms kernel [0.05, 0.25, 0.4, 0.25, 0.05](Kohn and Smith, 2005, Smith and Kohn, 2008) before further analysis.

We only included neuronal pairs with a geometric mean firing rate more than 0.5 spikes/sec for further analysis. We classified a CCG as significant if the peak of the jitter-corrected CCG occurred within 10ms of zero and was more than 7 standard deviations (SD) above the mean of the noise distribution, similar to previous studies(Siegle et al., 2021). The noise distribution for a CCG was defined as the flanks of the jittered-corrected CCG ($\{CCG(\tau)|100 \geq |\tau| \geq 50ms\}$). All analyses presented here involve only significant, jitter-corrected cross-correlograms. We also used a more stringent criteria in some analysis which requires the significant CCG peaks to be more than 10 SD than the CCG noise, to ensure than our results generalize across the choices of threshold (Figure S2).

To assess the directionality of functional interactions or signal flow between pair of neurons, we focused on two metrics derived from the CCG functions. One is the peak lag (PL), which describes the time lag of peak correlation between spike trains for neuron *k* (target) relative to neuron *j* (reference). PL is a positive value if reference neuron *j* leads target neuron *k* in spike timing and is negative if *j* lags *k*. PL is 0 if j and k firing synchronously. The second metric we

used to assess the signal flow is CCG asymmetry, which is computed by subtracting the sum of CCG values during [-13, 0]ms time window from the sum of CCG values during [0, 13]ms. Similar to PL, a positive CCG asymmetry indicates reference neuron *j* leads *k*, negative asymmetry indicates *j* lags *k*. The 13ms window was chosen as half of the 25ms jitter window as in previous studies(Jia et al., 2022). Compared to the peak lag, CCG asymmetry in addition captures the strength of the functional interactions between pairs of neurons and doesn't depend much on the exact CCG peak shape, which is usually more complicated for corticocortical functional interactions(Alonso and Martinez, 1998).

To determine whether border ownership selectivity (B_{own}) is predicted by the interlaminar signal flow, we built a generalized linear model (GLM). We focused on the four key interlaminar combinations (4C-2/3, 4A/B-2/3, 4C-5/6, 4A/B-5/6), where the latter laminar compartment receives feedback/horizontal input (FH_i). Only neuronal pairs exhibiting significant CCGs were included as individual samples in GLM. The resulting GLM was:

$$B_{own}(pair) \sim 1 + CCG\ asymmetry + \ CCG\ laminar\ combination$$

B_{own}(pair) was calculated as the geometric mean B_{own} for the neuronal pair with significant CCG. Specifically, $B_{own}(pair) = \sqrt{B_{own}(j) * B_{own}(k)}$, where $B_{own}(j)$ and $B_{own}(k)$ represents the modulation index for each constituent neuron *j* and *k*. We calculated the B_{own} for each orientation first, and then averaged across the 4 orientations on the absolute values.

Statistical Analyses

B_{own} for each neuron was assessed with ANOVA. The proportion of B_{own} neurons within different layers was assessed using chi-squared test of homogeneity. The sign of populational border ownership preferences from individual recording session was tested with sign test. The sign

of populational CCG peak lag for a given laminar compartment combination was assessed with sign test. The comparisons of peak lag and CCG asymmetry between CRF and nCRF stimulation condition for each laminar compartment combination were evaluated using Wilcoxon rank-sum tests. The dependence between CCG asymmetry and B_{own} for pair of neurons was assessed using GLM.

Acknowledgments.

We thank Tim Harris and Karel Svoboda for providing the Neuropixel probes, Jonathan C. Horton for extensive help with the recordings and histology, Jonathan Nassi for helpful comments on the results and interpretations, Danielle Lopes, Stephen Cital, Shellie Hyde and Sam Baker for technical assistance. This work was supported by NIH Grants EY014924, NS116623 and EY029759, and a Ben Barres Professorship to T.M.

Author Contributions

Conceptualization, S.Z., X.C. and T.M.; Investigation, S.Z., X.C. and T.M.; Software, S.Z. and E.T.; Formal Analysis, S.Z. and Y.J.O.; Visualization, S.Z., Y.J.O.; Writing – Original Draft, S.Z. and T.M.; Writing – Review and Editing, S.Z., Y.J.O., E.T., X.C., T.M.; Funding Acquisition, X.C. and T.M.

Declaration of Interests

The authors declare no competing interests.

Data and Code Availability

The data and custom code supporting this study will be made available online upon final publication.

References

ADESNIK, H., BRUNS, W., TANIGUCHI, H., HUANG, Z. J. & SCANZIANI, M. 2012. A neural circuit for spatial summation in visual cortex. *Nature,* 490**,** 226-31.

AERTSEN, A. M. & GERSTEIN, G. L. 1985. Evaluation of neuronal connectivity: sensitivity of cross-correlation. *Brain Res,* 340**,** 341-54.

ALBRIGHT, T. D. & STONER, G. R. 2002. Contextual influences on visual processing. *Annu Rev Neurosci,* 25**,** 339-79.

ALLMAN, J., MIEZIN, F. & MCGUINNESS, E. 1985. Stimulus specific responses from beyond the classical receptive field: neurophysiological mechanisms for local-global comparisons in visual neurons. *Annu Rev Neurosci,* 8**,** 407-30.

ALONSO, J. & CHEN, Y. 2009. Receptive field. *Scholarpedia,* 4**,** 5393.

ALONSO, J. M. & MARTINEZ, L. M. 1998. Functional connectivity between simple cells and complex cells in cat striate cortex. *Nature Neuroscience,* 1**,** 395-403.

ALONSO, J. M., USREY, W. M. & REID, R. C. 1996. Precisely correlated firing in cells of the lateral geniculate nucleus. *Nature,* 383**,** 815-9.

ANDERSON, J. C. & MARTIN, K. A. 2009. The synaptic connections between cortical areas V1 and V2 in macaque monkey. *J Neurosci,* 29**,** 11283-93.

ANDREWS, T. J., SCHLUPPECK, D., HOMFRAY, D., MATTHEWS, P. & BLAKEMORE, C. 2002. Activity in the fusiform gyrus predicts conscious perception of Rubin's vase-face illusion. *Neuroimage,* 17**,** 890-901.

ANGELUCCI, A., BIJANZADEH, M., NURMINEN, L., FEDERER, F., MERLIN, S. & BRESSLOFF, P. C. 2017. Circuits and Mechanisms for Surround Modulation in Visual Cortex. *Annu Rev Neurosci,* 40**,** 425-451.

ANGELUCCI, A. & BRESSLOFF, P. C. 2006. Contribution of feedforward, lateral and feedback connections to the classical receptive field center and extra-classical receptive field surround of primate V1 neurons. *Prog Brain Res,* 154**,** 93-120.

ANGELUCCI, A., LEVITT, J. B., WALTON, E. J., HUPE, J. M., BULLIER, J. & LUND, J. S. 2002. Circuits for local and global signal integration in primary visual cortex. *J Neurosci,* 22**,** 8633-46.

BAIR, W., CAVANAUGH, J. R. & MOVSHON, J. A. 2003. Time course and time-distance relationships for surround suppression in macaque V1 neurons. *J Neurosci,* 23**,** 7690-701.

BAIR, W., ZOHARY, E. & NEWSOME, W. T. 2001. Correlated firing in macaque visual area MT: time scales and relationship to behavior. *J Neurosci,* 21**,** 1676-97.

BLASDEL, G. G. & LUND, J. S. 1983. Termination of afferent axons in macaque striate cortex. *J Neurosci,* 3**,** 1389-413.

BRIGGS, F., MANGUN, G. R. & USREY, W. M. 2013. Attention enhances synaptic efficacy and the signal-to-noise ratio in neural circuits. *Nature,* 499**,** 476-80.

BRINGUIER, V., CHAVANE, F., GLAESER, L. & FREGNAC, Y. 1999. Horizontal propagation of visual activity in the synaptic integration field of area 17 neurons. *Science,* 283**,** 695-9.

BULLIER, J., HUPE, J. M., JAMES, A. C. & GIRARD, P. 2001. The role of feedback connections in shaping the responses of visual cortical neurons. *Prog Brain Res,* 134**,** 193-204.

CALLAWAY, E. M. 1998. Local circuits in primary visual cortex of the macaque monkey. *Annu Rev Neurosci,* 21**,** 47-74.

CALLAWAY, E. M. 2004. Feedforward, feedback and inhibitory connections in primate visual cortex. *Neural Netw,* 17**,** 625-32.

CHEN, M., YAN, Y., GONG, X., GILBERT, C. D., LIANG, H. & LI, W. 2014. Incremental integration of global contours through interplay between visual cortical areas. *Neuron,* 82**,** 682-94.

CHEN, R., WANG, F., LIANG, H. & LI, W. 2017. Synergistic Processing of Visual Contours across Cortical Layers in V1 and V2. *Neuron,* 96**,** 1388-1402 e4.

CHISUM, H. J., MOOSER, F. & FITZPATRICK, D. 2003. Emergent properties of layer 2/3 neurons reflect the collinear arrangement of horizontal connections in tree shrew visual cortex. *J Neurosci,* 23**,** 2947-60.

CHU, C. C., CHIEN, P. F. & HUNG, C. P. 2014. Tuning dissimilarity explains short distance decline of spontaneous spike correlation in macaque V1. *Vision Res,* 96**,** 113-32.

CRAFT, E., SCHÜTZE, H., NIEBUR, E. & VON DER HEYDT, R. 2007. A neural model of figure-ground organization. *J. Neurophysiol,* 97**,** 4310-4326.

DENMAN, D. J. & CONTRERAS, D. 2014. The structure of pairwise correlation in mouse primary visual cortex reveals functional organization in the absence of an orientation map. *Cereb Cortex,* 24**,** 2707-20.

EGUCHI, A. & STRINGER, S. M. 2016. Neural network model develops border ownership representation through visually guided learning. *Neurobiol Learn Mem,* 136**,** 147-165.

FANG, F., BOYACI, H. & KERSTEN, D. 2009. Border ownership selectivity in human early visual cortex and its modulation by attention. *J Neurosci,* 29**,** 460-5.

FEDERER, F., TA'AFUA, S., MERLIN, S., HASSANPOUR, M. S. & ANGELUCCI, A. 2021. Stream-specific feedback inputs to the primate primary visual cortex. *Nat Commun,* 12**,** 228.

FITZPATRICK, D. 2000. Seeing beyond the receptive field in primary visual cortex. *Curr Opin Neurobiol,* 10**,** 438-43.

FRANKEN, T. P. & REYNOLDS, J. H. 2021. Columnar processing of border ownership in primate visual cortex. *Elife,* 10.

GIESELMANN, M. A. & THIELE, A. 2022. Stimulus dependence of directed information exchange between cortical layers in macaque V1. *Elife,* 11.

GILBERT, C. D. & WIESEL, T. N. 1983. Clustered intrinsic connections in cat visual cortex. *J Neurosci,* 3**,** 1116-33.

GILBERT, C. D. & WIESEL, T. N. 1990. The influence of contextual stimuli on the orientation selectivity of cells in primary visual cortex of the cat. *Vision Res,* 30**,** 1689-701.

GIRARD, P., HUPE, J. M. & BULLIER, J. 2001. Feedforward and feedback connections between areas V1 and V2 of the monkey have similar rapid conduction velocities. *J Neurophysiol,* 85**,** 1328-31.

GRINVALD, A., LIEKE, E. E., FROSTIG, R. D. & HILDESHEIM, R. 1994. Cortical point-spread function and long-range lateral interactions revealed by real-time optical imaging of macaque monkey primary visual cortex. *J Neurosci,* 14**,** 2545-68.

GUR, M., KAGAN, I. & SNODDERLY, D. M. 2005. Orientation and direction selectivity of neurons in V1 of alert monkeys: functional relationships and laminar distributions. *Cereb Cortex,* 15**,** 1207-21.

HANSEN, B. J., CHELARU, M. I. & DRAGOI, V. 2012. Correlated variability in laminar cortical circuits. *Neuron,* 76**,** 590-602.

HARRISON, M. T. & GEMAN, S. 2009. A rate and history-preserving resampling algorithm for neural spike trains. *Neural Comput,* 21**,** 1244-58.

HARTLINE, H. K. 1938. THE RESPONSE OF SINGLE OPTIC NERVE FIBERS OF THE VERTEBRATE EYE TO ILLUMINATION OF THE RETINA. *American Journal of Physiology-Legacy Content,* 121**,** 400-415.

HEMBROOK-SHORT, J. R., MOCK, V. L., USREY, W. M. & BRIGGS, F. 2019. Attention Enhances the Efficacy of Communication in V1 Local Circuits. *J Neurosci,* 39**,** 1066-1076.

HENDRICKSON, A. E., WILSON, J. R. & OGREN, M. P. 1978. The neuroanatomical organization of pathways between the dorsal lateral geniculate nucleus and visual cortex in Old World and New World primates. *J Comp Neurol,* 182**,** 123-36.

HENRY, C. A., JOSHI, S., XING, D., SHAPLEY, R. M. & HAWKEN, M. J. 2013. Functional characterization of the extraclassical receptive field in macaque V1: contrast, orientation, and temporal dynamics. *J Neurosci,* 33**,** 6230-42.

HESSE, J. K. & TSAO, D. Y. 2016. Consistency of Border-Ownership Cells across Artificial Stimuli, Natural Stimuli, and Stimuli with Ambiguous Contours. *J Neurosci,* 36**,** 11338-11349.

HESSE, J. K. & TSAO, D. Y. 2023. Functional modules for visual scene segmentation in macaque visual cortex. *Proc Natl Acad Sci U S A,* 120**,** e2221122120.

HIRABAYASHI, T. & MIYASHITA, Y. 2005. Dynamically modulated spike correlation in monkey inferior temporal cortex depending on the feature configuration within a whole object. *J Neurosci,* 25**,** 10299-307.

HIRABAYASHI, T., TAKEUCHI, D., TAMURA, K. & MIYASHITA, Y. 2010. Triphasic dynamics of stimulus-dependent information flow between single neurons in macaque inferior temporal cortex. *J Neurosci,* 30**,** 10407-21.

HUBEL, D. H. & WIESEL, T. N. 1972. Laminar and columnar distribution of geniculo-cortical fibers in the macaque monkey. *J Comp Neurol,* 146**,** 421-50.

HUNG, C. P., RAMSDEN, B. M. & ROE, A. W. 2007. A functional circuitry for edge-induced brightness perception. *Nat Neurosci,* 10**,** 1185-90.

HUPE, J. M., JAMES, A. C., GIRARD, P., LOMBER, S. G., PAYNE, B. R. & BULLIER, J. 2001. Feedback connections act on the early part of the responses in monkey visual cortex. *J Neurophysiol,* 85**,** 134-45.

HUPE, J. M., JAMES, A. C., PAYNE, B. R., LOMBER, S. G., GIRARD, P. & BULLIER, J. 1998. Cortical feedback improves discrimination between figure and background by V1, V2 and V3 neurons. *Nature,* 394**,** 784-7.

ICHIDA, J. M., SCHWABE, L., BRESSLOFF, P. C. & ANGELUCCI, A. 2007. Response facilitation from the "suppressive" receptive field surround of macaque V1 neurons. *J Neurophysiol,* 98**,** 2168-81.

JEHEE, J. F., LAMME, V. A. & ROELFSEMA, P. R. 2007. Boundary assignment in a recurrent network architecture. *Vision Res,* 47**,** 1153-65.

JEURISSEN, D., SELF, M. W. & ROELFSEMA, P. R. 2016. Serial grouping of 2D-image regions with object-based attention in humans. *Elife,* 5.

JIA, X., TANABE, S. & KOHN, A. 2013. gamma and the coordination of spiking activity in early visual cortex. *Neuron,* 77**,** 762-74.

JIA, X. X., SIEGLE, J. H., DURAND, S., HELLER, G., RAMIREZ, T. K., KOCH, C. & OLSEN, S. R. 2022. Multi-regional module-based signal transmission in mouse visual cortex. *Neuron,* 110**,** 1585-+.

JUN, J. J., STEINMETZ, N. A., SIEGLE, J. H., DENMAN, D. J., BAUZA, M., BARBARITS, B., LEE, A. K., ANASTASSIOU, C. A., ANDREI, A., AYDIN, C., BARBIC, M., BLANCHE, T. J., BONIN, V., COUTO, J., DUTTA, B., GRATIY, S. L., GUTNISKY, D. A., HAUSSER, M., KARSH, B., LEDOCHOWITSCH, P., LOPEZ, C. M., MITELUT, C., MUSA, S., OKUN, M., PACHITARIU, M., PUTZEYS, J., RICH, P. D., ROSSANT, C., SUN, W. L., SVOBODA, K., CARANDINI, M., HARRIS, K. D., KOCH, C., O'KEEFE, J. & HARRIS, T. D. 2017. Fully integrated silicon probes for high-density recording of neural activity. *Nature,* 551**,** 232-236.

KAPADIA, M. K., ITO, M., GILBERT, C. D. & WESTHEIMER, G. 1995. Improvement in visual sensitivity by changes in local context: parallel studies in human observers and in V1 of alert monkeys. *Neuron,* 15**,** 843-56.

KELLER, A. J., ROTH, M. M. & SCANZIANI, M. 2020. Feedback generates a second receptive field in neurons of the visual cortex. *Nature,* 582**,** 545-549.

KLEINER, M., BRAINARD, D. & PELLI, D. 2007. What's new in Psychtoolbox-3? *Perception,* 36**,** 14-14.

KLINK, P. C., DAGNINO, B., GARIEL-MATHIS, M. A. & ROELFSEMA, P. R. 2017. Distinct Feedforward and Feedback Effects of Microstimulation in Visual Cortex Reveal Neural Mechanisms of Texture Segregation. *Neuron,* 95**,** 209-220 e3.

KNIERIM, J. J. & VAN ESSEN, D. C. 1992. Neuronal responses to static texture patterns in area V1 of the alert macaque monkey. *J Neurophysiol,* 67**,** 961-80.

KOGO, N., STRECHA, C., VAN GOOL, L. & WAGEMANS, J. 2010. Surface construction by a 2-D differentiation-integration process: a neurocomputational model for perceived border ownership, depth, and lightness in Kanizsa figures. *Psychol Rev,* 117**,** 406-39.

KOHN, A. & SMITH, M. A. 2005. Stimulus dependence of neuronal correlation in primary visual cortex of the macaque. *J Neurosci,* 25**,** 3661-73.

KOURTZI, Z. & KANWISHER, N. 2001. Representation of perceived object shape by the human lateral occipital complex. *Science,* 293**,** 1506-9.

LAMME, V. A. 1995. The neurophysiology of figure-ground segregation in primary visual cortex. *J Neurosci,* 15**,** 1605-15.

LAMME, V. A., ZIPSER, K. & SPEKREIJSE, H. 1998. Figure-ground activity in primary visual cortex is suppressed by anesthesia. *Proc Natl Acad Sci U S A,* 95**,** 3263-8.

LAYTON, O. W., MINGOLLA, E. & YAZDANBAKHSH, A. 2012. Dynamic coding of border-ownership in visual cortex. *J Vis,* 12**,** 8.

LEE, T. S., YANG, C. F., ROMERO, R. D. & MUMFORD, D. 2002. Neural activity in early visual cortex reflects behavioral experience and higher-order perceptual saliency. *Nat Neurosci,* 5**,** 589-97.

LI, W., PIECH, V. & GILBERT, C. D. 2006. Contour saliency in primary visual cortex. *Neuron,* 50**,** 951-62.

LI, Y., WANG, T., YANG, Y., DAI, W., WU, Y., LI, L., HAN, C., ZHONG, L., LI, L., WANG, G., DOU, F. & XING, D. 2022. Cascaded normalizations for spatial integration in the primary visual cortex of primates. *Cell Rep,* 40**,** 111221.

LIANG, H., GONG, X., CHEN, M., YAN, Y., LI, W. & GILBERT, C. D. 2017. Interactions between feedback and lateral connections in the primary visual cortex. *Proc Natl Acad Sci U S A,* 114**,** 8637-8642.

LUND, J. S. 1973. Organization of neurons in the visual cortex, area 17, of the monkey (Macaca mulatta). *J Comp Neurol,* 147**,** 455-96.

MARKOV, N. T., VEZOLI, J., CHAMEAU, P., FALCHIER, A., QUILODRAN, R., HUISSOUD, C., LAMY, C., MISERY, P., GIROUD, P., ULLMAN, S., BARONE, P., DEHAY, C., KNOBLAUCH, K. & KENNEDY, H. 2014. Anatomy of hierarchy: feedforward and feedback pathways in macaque visual cortex. *J Comp Neurol,* 522**,** 225-59.

MARTIN, A. B. & VON DER HEYDT, R. 2015. Spike synchrony reveals emergence of proto-objects in visual cortex. *Journal of Neuroscience,* 35**,** 6860-6870.

MEHRANI, P. & TSOTSOS, J. K. 2021. Early recurrence enables figure border ownership. *Vision Res,* 186**,** 23-33.

MELSSEN, W. J. & EPPING, W. J. 1987. Detection and estimation of neural connectivity based on crosscorrelation analysis. *Biol Cybern,* 57**,** 403-14.

MOORE, G. P., SEGUNDO, J. P., PERKEL, D. H. & LEVITAN, H. 1970. Statistical signs of synaptic interaction in neurons. *Biophys J,* 10**,** 876-900.

MULLER, J. R., METHA, A. B., KRAUSKOPF, J. & LENNIE, P. 2003. Local signals from beyond the receptive fields of striate cortical neurons. *J Neurophysiol,* 90**,** 822-31.

NAKAYAMA, K., HE, Z. J. & SHIMOJO, S. 1995. Visual Surface Representation: A Critical Link between Lower-Level and Higher-Level Vision. *In:* KOSSLYN, S. M. & OSHERSON, D. N. (eds.) *An Invitation to Cognitive Science, Volume 2: Visual Cognition.* The MIT Press.

NANDY, A. S., NASSI, J. J. & REYNOLDS, J. H. 2017. Laminar Organization of Attentional Modulation in Macaque Visual Area V4. *Neuron,* 93**,** 235-246.

NASSI, J. J., LOMBER, S. G. & BORN, R. T. 2013. Corticocortical feedback contributes to surround suppression in V1 of the alert primate. *J Neurosci,* 33**,** 8504-17.

NELSON, J. I. & FROST, B. J. 1985. Intracortical facilitation among co-oriented, co-axially aligned simple cells in cat striate cortex. *Exp Brain Res,* 61**,** 54-61.

NELSON, J. I., SALIN, P. A., MUNK, M. H., ARZI, M. & BULLIER, J. 1992. Spatial and temporal coherence in cortico-cortical connections: a cross-correlation study in areas 17 and 18 in the cat. *Vis Neurosci,* 9**,** 21-37.

NICHOLSON, C. & FREEMAN, J. A. 1975. Theory of current source-density analysis and determination of conductivity tensor for anuran cerebellum. *J Neurophysiol,* 38**,** 356-68.

NOTHDURFT, H. C., GALLANT, J. L. & VAN ESSEN, D. C. 1999. Response modulation by texture surround in primate area V1: correlates of "popout" under anesthesia. *Vis Neurosci,* 16**,** 15-34.

NURMINEN, L., MERLIN, S., BIJANZADEH, M., FEDERER, F. & ANGELUCCI, A. 2018. Top-down feedback controls spatial summation and response amplitude in primate visual cortex. *Nat Commun,* 9**,** 2281.

O'KUSKY, J. & COLONNIER, M. 1982. A laminar analysis of the number of neurons, glia, and synapses in the adult cortex (area 17) of adult macaque monkeys. *J Comp Neurol,* 210**,** 278-90.

OSTOJIC, S., BRUNEL, N. & HAKIM, V. 2009. How connectivity, background activity, and synaptic properties shape the cross-correlation between spike trains. *J Neurosci,* 29**,** 10234-53.

PAK, A., RYU, E., LI, C. & CHUBYKIN, A. A. 2020. Top-Down Feedback Controls the Cortical Representation of Illusory Contours in Mouse Primary Visual Cortex. *J Neurosci,* 40**,** 648-660.

PERKEL, D. H., GERSTEIN, G. L. & MOORE, G. P. 1967. Neuronal spike trains and stochastic point processes. II. Simultaneous spike trains. *Biophys J,* 7**,** 419-40.

PETTINE, W. W., STEINMETZ, N. A. & MOORE, T. 2019. Laminar segregation of sensory coding and behavioral readout in macaque V4. *Proc Natl Acad Sci U S A,* 116**,** 14749-14754.

POORT, J., RAUDIES, F., WANNIG, A., LAMME, V. A., NEUMANN, H. & ROELFSEMA, P. R. 2012. The role of attention in figure-ground segregation in areas V1 and V4 of the visual cortex. *Neuron,* 75**,** 143-56.

QIU, F. T., SUGIHARA, T. & VON DER HEYDT, R. 2007. Figure-ground mechanisms provide structure for selective attention. *Nature Neuroscience,* 10**,** 1492-1499.

RAMSDEN, B. M., HUNG, C. P. & ROE, A. W. 2001. Real and illusory contour processing in area V1 of the primate: a cortical balancing act. *Cereb Cortex,* 11**,** 648-65.

REID, R. C. & ALONSO, J. M. 1995. Specificity of monosynaptic connections from thalamus to visual cortex. *Nature,* 378**,** 281-4.

ROCKLAND, K. S. & LUND, J. S. 1983. Intrinsic laminar lattice connections in primate visual cortex. *J Comp Neurol,* 216**,** 303-18.

ROCKLAND, K. S. & PANDYA, D. N. 1979. Laminar origins and terminations of cortical connections of the occipital lobe in the rhesus monkey. *Brain Res,* 179**,** 3-20.

ROCKLAND, K. S., SALEEM, K. S. & TANAKA, K. 1994. Divergent feedback connections from areas V4 and TEO in the macaque. *Vis Neurosci,* 11**,** 579-600.

ROCKLAND, K. S. & VIRGA, A. 1989. Terminal arbors of individual "feedback" axons projecting from area V2 to V1 in the macaque monkey: a study using immunohistochemistry of anterogradely transported Phaseolus vulgaris-leucoagglutinin. *J Comp Neurol,* 285**,** 54-72.

ROE, A. W. & TS'O, D. Y. 1999. Specificity of color connectivity between primate V1 and V2. *J Neurophysiol,* 82**,** 2719-30.

ROELFSEMA, P. R. 2006. Cortical algorithms for perceptual grouping. *Annu Rev Neurosci,* 29**,** 203-27.

SAKAI, K. & NISHIMURA, H. 2006. Surrounding suppression and facilitation in the determination of border ownership. *J Cogn Neurosci,* 18**,** 562-79.

SCHWABE, L., OBERMAYER, K., ANGELUCCI, A. & BRESSLOFF, P. C. 2006. The role of feedback in shaping the extra-classical receptive field of cortical neurons: a recurrent network model. *J Neurosci,* 26**,** 9117-29.

SCHWARZ, C. & BOLZ, J. 1991. Functional specificity of a long-range horizontal connection in cat visual cortex: a cross-correlation study. *J Neurosci,* 11**,** 2995-3007.

SELF, M. W., JEURISSEN, D., VAN HAM, A. F., VAN VUGT, B., POORT, J. & ROELFSEMA, P. R. 2019. The Segmentation of Proto-Objects in the Monkey Primary Visual Cortex. *Curr Biol,* 29**,** 1019-1029 e4.

SELF, M. W., VAN KERKOERLE, T., SUPER, H. & ROELFSEMA, P. R. 2013. Distinct roles of the cortical layers of area V1 in figure-ground segregation. *Curr Biol,* 23**,** 2121-9.

SENZAI, Y., FERNANDEZ-RUIZ, A. & BUZSAKI, G. 2019. Layer-Specific Physiological Features and Interlaminar Interactions in the Primary Visual Cortex of the Mouse. *Neuron,* 101**,** 500-513 e5.

SHMUEL, A., KORMAN, M., STERKIN, A., HAREL, M., ULLMAN, S., MALACH, R. & GRINVALD, A. 2005. Retinotopic axis specificity and selective clustering of feedback projections from V2 to V1 in the owl monkey. *J Neurosci,* 25**,** 2117-31.

SIBILLE, J., GEHR, C., BENICHOV, J. I., BALASUBRAMANIAN, H., TEH, K. L., LUPASHINA, T., VALLENTIN, D. & KREMKOW, J. 2022. High-density electrode recordings reveal strong and specific connections between retinal ganglion cells and midbrain neurons. *Nature Communications,* 13.

SIEGLE, J. H., JIA, X., DURAND, S., GALE, S., BENNETT, C., GRADDIS, N., HELLER, G., RAMIREZ, T. K., CHOI, H., LUVIANO, J. A., GROBLEWSKI, P. A., AHMED, R., ARKHIPOV, A., BERNARD, A., BILLEH, Y. N., BROWN, D., BUICE, M. A., CAIN, N., CALDEJON, S., CASAL, L., CHO, A., CHVILICEK, M., COX, T. C., DAI, K., DENMAN, D. J., DE VRIES, S. E. J., DIETZMAN, R., ESPOSITO, L., FARRELL, C., FENG, D., GALBRAITH, J., GARRETT, M., GELFAND, E. C., HANCOCK, N., HARRIS, J. A., HOWARD, R., HU, B., HYTNEN, R., IYER, R., JESSETT, E., JOHNSON, K., KATO, I., KIGGINS, J., LAMBERT, S., LECOQ, J., LEDOCHOWITSCH, P., LEE, J. H., LEON, A., LI, Y., LIANG, E., LONG, F., MACE, K., MELCHIOR, J., MILLMAN, D., MOLLENKOPF, T., NAYAN, C., NG, L., NGO, K., NGUYEN, T., NICOVICH, P. R., NORTH, K., OCKER, G. K., OLLERENSHAW, D., OLIVER, M., PACHITARIU, M., PERKINS, J., REDING, M., REID, D., ROBERTSON, M., RONELLENFITCH, K., SEID, S., SLAUGHTERBECK, C., STOECKLIN, M., SULLIVAN, D., SUTTON, B., SWAPP, J., THOMPSON, C., TURNER, K., WAKEMAN, W., WHITESELL, J. D., WILLIAMS, D., WILLIFORD, A., YOUNG, R., ZENG, H., NAYLOR, S., PHILLIPS, J. W., REID, R. C., MIHALAS, S., OLSEN, S. R. & KOCH, C. 2021. Survey of spiking in the mouse visual system reveals functional hierarchy. *Nature,* 592**,** 86-92.

SILLITO, A. M., GRIEVE, K. L., JONES, H. E., CUDEIRO, J. & DAVIS, J. 1995. Visual cortical mechanisms detecting focal orientation discontinuities. *Nature,* 378**,** 492-6.

SMITH, M. A. & KOHN, A. 2008. Spatial and temporal scales of neuronal correlation in primary visual cortex. *J Neurosci,* 28**,** 12591-603.

STEINMETZ, P. N., ROY, A., FITZGERALD, P. J., HSIAO, S. S., JOHNSON, K. O. & NIEBUR, E. 2000. Attention modulates synchronized neuronal firing in primate somatosensory cortex. *Nature,* 404**,** 187-90.

STETTLER, D. D., DAS, A., BENNETT, J. & GILBERT, C. D. 2002. Lateral connectivity and contextual interactions in macaque primary visual cortex. *Neuron,* 36**,** 739-50.

SUGIHARA, T., QIU, F. T. & VON DER HEYDT, R. 2011. The speed of context integration in the visual cortex. *J Neurophysiol,* 106**,** 374-85.

SUPER, H., ROMEO, A. & KEIL, M. 2010. Feed-forward segmentation of figure-ground and assignment of border-ownership. *PLoS One,* 5**,** e10705.

SUPER, H., SPEKREIJSE, H. & LAMME, V. A. 2001. Two distinct modes of sensory processing observed in monkey primary visual cortex (V1). *Nat Neurosci,* 4**,** 304-10.

SWINDALE, N. V. 1998. Orientation tuning curves: empirical description and estimation of parameters. *Biol Cybern,* 78**,** 45-56.

TOOTELL, R. B., SWITKES, E., SILVERMAN, M. S. & HAMILTON, S. L. 1988. Functional anatomy of macaque striate cortex. II. Retinotopic organization. *J Neurosci,* 8**,** 1531-68.

TRAUTMANN, E. M., HESSE, J. K., STINE, G. M., XIA, R., ZHU, S., O'SHEA, D. J., KARSH, B., COLONELL, J., LANFRANCHI, F. F., VYAS, S., ZIMNIK, A., STEINMANN, N. A., WAGENAAR, D. A., ANDREI, A., LOPEZ, C. M., O'CALLAGHAN, J., PUTZEYS, J., RADUCANU, B. C., WELKENHUYSEN, M., CHURCHLAND, M., MOORE, T., SHADLEN, M., SHENOY, K., TSAO, D., DUTTA, B. & HARRIS, T. 2023. Large-scale high-density brain-wide neural recording in nonhuman primates. *bioRxiv***,** 2023.02.01.526664.

TREPKA, E. B., ZHU, S. D., XIA, R. B., CHEN, X. M. & MOORE, T. 2022. Functional interactions among neurons within single columns of macaque V1. *Elife,* 11.

TS'O, D. Y., GILBERT, C. D. & WIESEL, T. N. 1986. Relationships between horizontal interactions and functional architecture in cat striate cortex as revealed by cross-correlation analysis. *J Neurosci,* 6**,** 1160-70.

USREY, W. M., REPPAS, J. B. & REID, R. C. 1998. Paired-spike interactions and synaptic efficacy of retinal inputs to the thalamus. *Nature,* 395**,** 384-7.

VAN KERKOERLE, T., SELF, M. W., DAGNINO, B., GARIEL-MATHIS, M. A., POORT, J., VAN DER TOGT, C. & ROELFSEMA, P. R. 2014. Alpha and gamma oscillations characterize feedback and feedforward processing in monkey visual cortex. *Proc Natl Acad Sci U S A,* 111**,** 14332-41.

VAN KERKOERLE, T., SELF, M. W. & ROELFSEMA, P. R. 2017. Layer-specificity in the effects of attention and working memory on activity in primary visual cortex. *Nat Commun,* 8**,** 13804.

VANGENEUGDEN, J., VAN BEEST, E. H., COHEN, M. X., LORTEIJE, J. A. M., MUKHERJEE, S., KIRCHBERGER, L., MONTIJN, J. S., THAMIZHARASU, P., CAMILLO, D., LEVELT, C. N., ROELFSEMA, P. R., SELF, M. W. & HEIMEL, J. A. 2019. Activity in Lateral Visual Areas Contributes to Surround Suppression in Awake Mouse V1. *Curr Biol,* 29**,** 4268-4275 e7.

VON DER HEYDT, R. 2015. Figure-ground organization and the emergence of proto-objects in the visual cortex. *Frontiers in Psychology,* 6**,** 1695.

VON DER HEYDT, R. 2023. Visual cortical processing—From image to object representation. *Frontiers in Computer Science,* 5.

VON DER HEYDT, R., PETERHANS, E. & BAUMGARTNER, G. 1984. Illusory contours and cortical neuron responses. *Science,* 224**,** 1260-2.

WAGATSUMA, N., HU, B., VON DER HEYDT, R. & NIEBUR, E. 2021. Analysis of spiking synchrony in visual cortex reveals distinct types of top-down modulation signals for spatial and object-based attention. *PLoS Comput Biol,* 17**,** e1008829.

WALKER, G. A., OHZAWA, I. & FREEMAN, R. D. 1999. Asymmetric suppression outside the classical receptive field of the visual cortex. *J Neurosci,* 19**,** 10536-53.

WEBB, B. S., TINSLEY, C. J., BARRACLOUGH, N. E., PARKER, A. & DERRINGTON, A. M. 2003. Gain control from beyond the classical receptive field in primate primary visual cortex. *Vis Neurosci,* 20**,** 221-30.

WILLIFORD, J. R. & VON DER HEYDT, R. 2016. Figure-Ground Organization in Visual Cortex for Natural Scenes. *eNeuro,* 3.

YAN, Y., ZHAOPING, L. & LI, W. 2018. Bottom-up saliency and top-down learning in the primary visual cortex of monkeys. *Proc Natl Acad Sci U S A,* 115**,** 10499-10504.

ZARELLA, M. D. & TS'O, D. Y. 2016. Cue combination encoding via contextual modulation of V1 and V2 neurons. *Eye Brain,* 8**,** 177-193.

ZHANG, N. R. & VON DER HEYDT, R. 2010. Analysis of the context integration mechanisms underlying figure-ground organization in the visual cortex. *Journal of Neuroscience,* 30**,** 6482-6496.

ZHANG, S., XU, M., KAMIGAKI, T., HOANG DO, J. P., CHANG, W. C., JENVAY, S., MIYAMICHI, K., LUO, L. & DAN, Y. 2014. Selective attention. Long-range and local circuits for top-down modulation of visual cortex processing. *Science,* 345**,** 660-5.

ZHAOPING, L. 2005. Border ownership from intracortical interactions in visual area v2. *Neuron,* 47**,** 143-53.

ZHOU, H., FRIEDMAN, H. S. & VON DER HEYDT, R. 2000. Coding of border ownership in monkey visual cortex. *J Neurosci,* 20**,** 6594-611.

ZHU, S. D., ZHANG, L. A. & VON DER HEYDT, R. 2020. Searching for object pointers in the visual cortex. *Journal of Neurophysiology,* 123**,** 1979-1994.

ZIPSER, K., LAMME, V. A. & SCHILLER, P. H. 1996. Contextual modulation in primary visual cortex. *J Neurosci,* 16**,** 7376-89.

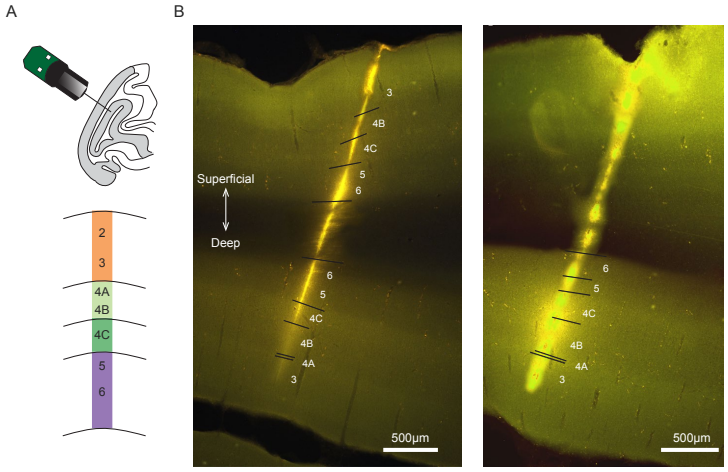

Figure S1. Histological data for Neuropixels recordings in macaque V1.
(A). Neuropixels probe (384 channels/3.84mm) penetrations made into the lateral surface and underlying calcarine sulcus of macaque V1. Lower, diagram of designated laminar compartments. (B). Histological reconstructed electrode tracks based on DiI staining for two example recordings (*pen3*, *pen 4,* M2). Here Neuropixels probes passed lateral surface and reached to the calcarine sulcus of V1. Neurons in the calcarine sulcus of V1 in those two recordings were tested and included in the analysis. Designated boundaries were shown. Scales bar, 500 µm.

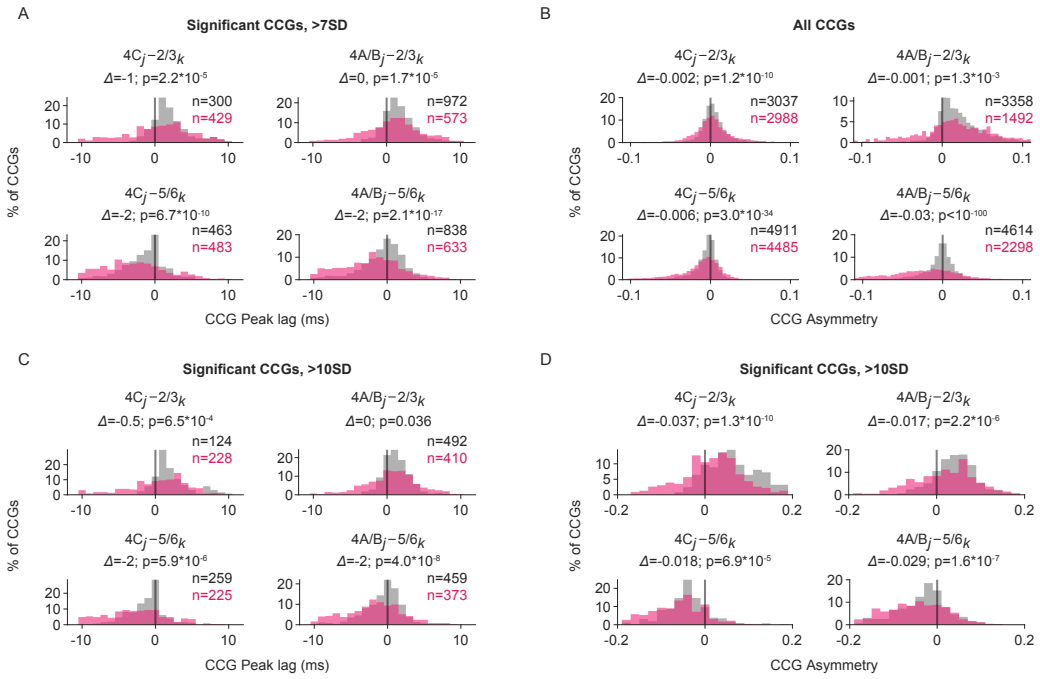

Figure S2. Shift in relative spiking time across sessions between CRF and nCRF stimulation for different CCG significance criteria.
(A). Shift of CCG peak lag for combined dataset for each of the 4 key interlaminar combinations. Histograms distributions of CCG peak lag for all significant CCGs during CRF (gray) and nCRF (magenta) stimulation. Δ denotes the populational median shift for CCG peak lag during nCRF stimulation relative to CRF stimulation. Significant CCGs are defined as CCGs with peaks greater than 7SD of CCG noise (flank). (B). Similar to (A), instead of CCG peak lags, compared are CCG asymmetry for all CCGs (both significant and non-significant CCGs). (C). same as (A). Instead of 7SD, significant CCGs are defined as CCGs with peaks greater than 7SD of CCG noise (flank). (D). same as (C). Instead of CCG peak lags, compared are CCG asymmetry.

Table S1. GLM model for dependence of border ownership modulation on CCG asymmetry.

B_{own}(pair)	Estimate	SE	tStat	pValue
Intercept	0.15	0.0025	60.2	0
CCG asymmetry	-0.10	0.016	-6.3	$4.0*10^{-10}$
Laminar (4C-5/6)	0.02	0.0036	5.5	$5.5*10^{-8}$
Laminar (4A/B-2/3)	-0.001	0.0033	-0.32	0.75
Laminar (4A/B-5/6)	0.018	0.0034	5.1	$3.8*10^{-7}$

Number of observations: 2118; Error degrees of freedom: 2113; R^2=0.078; F-statistic vs. constant model: 44.6, p-value=$5.8*10^{-36}$.